JOURNAL OF COMPUTATIONAL PHYSICS 81, 300–318 (1989)

A Numerical Study of Nonlinear Waves Arising in a One-Dimensional Model of a Fluidized Bed

IAN CHRISTIE AND G. H. GANSER

Department of Mathematics, West Virginia University, Morgantown, West Virginia 26506

Received February 26, 1987; revised March 30, 1988

A third-order nonlinear problem, which under certain circumstances approximates the flow in a 1-dimensional fluidized bed, is solved numerically. A Petrov–Galerkin finite element method, with piecewise linear trial functions and cubic spline test functions, is used for the discretization in space. If product approximation is applied to the numerical representation of the nonlinear terms, then the scheme is fourth-order in space in the finite difference sense. Second-order backward differentiation is used for the time stepping. It is found that, while certain values of the time step may produce stable results, a reduction in the time step introduces instability. This is confirmed by a von Neumann stability analysis of a simplified case and is also shown to be reasonable in view of the continuous problem which contains stable and unstable modes. A set of numerical experiments is presented.

1. INTRODUCTION

The system of partial differential equations

$$\alpha_t + (\alpha u)_x = 0 \tag{1a}$$

$$\alpha u + (1-\alpha)\, v = j \tag{1b}$$

$$\alpha(1-\alpha)\,\rho(u_t + uu_x) = B(\alpha)(v-u) - (1-\alpha)(\alpha\beta(\alpha))_x - \alpha(1-\alpha)\, g\rho + 2\mu(1-\alpha)(\alpha u_x)_x \tag{1c}$$

approximates the 1-dimensional vertical flow in a fluidized bed where x is the vertical coordinate and t is time. The function $\alpha(x, t)$ is the concentration of the particles by volume. The velocities of the particle and fluid phases are denoted by u and v, while j and μ are constants representing the volumetric flux, and the viscosity of the particle phase, respectively. The function

$$B(\alpha) = \alpha(1-\alpha)^{2-n} K$$

is the coefficient of friction between the two phases, where $K = 9\mu_g/2R^2$, μ_g is the viscosity of the gas, and R is the radius of the particles. For our purposes, a more convenient form is $K = g\rho/v_\infty$, where v_∞ is the terminal velocity of an isolated

0021-9991/89 $3.00

particle. The particle density is ρ and g is the acceleration due to gravity. Typical values for n are about 3 or 4. Little is known about the function $\alpha\beta(\alpha)$ which is related to the particle pressure and plays an important role in the study of stability of (1). We assume that the derivative of this function with respect to $1-\alpha$ is a linear function $-G(\alpha)>0$. The system above is a typical model of dispersed two-phase flow, see for example Needham and Merkin [10], Drew [2], and Homsy, El-Kaissy, and Didwania [5].

Under certain restrictions, such as the long wavelength and small amplitude approximations, the equation (Ganser and Drew [4], Liu [7])

$$\alpha_t - 2Na\alpha\alpha_x + R_2^{-1}\alpha_{xxx} + c_{0-}v[c_{0+}\alpha_{xx} + \tilde{c}_{0+}a(\alpha\alpha_x)_x + \alpha_{tx}] = 0 \tag{2}$$

can be regarded as an approximation to the system (1), where $a\alpha$ now denotes the value perturbed from the equilibrium state α_0. The coefficients are given as

$$\begin{aligned} B_0 &= B(\alpha_0) \\ G_0 &= G(\alpha_0) \\ R_2^{-1} &= (L_1/L)^2 \\ v &= L_c/L \\ c_{0\pm} &= -\alpha_0 n \pm \frac{1}{v_\infty(1+\alpha_0)^{n-1}}\sqrt{-G_0/\rho}. \end{aligned} \tag{3}$$

Here, L_1 and L_c are physical lengths, determined by the parameters in the problem, and L is the length scale related to the perturbations in the particle concentration. In addition, the term $\tilde{c}_{0+}a\alpha$ is related to the nonlinear correction to the speed of sound in the particle phase and $-2Na\alpha$ is the nonlinear correction to the speed of the continuity wave. In terms of the notation introduced in (1) these terms are determined by the formulas

$$\tilde{c}_{0+} = n + \frac{G_0'}{2v_\infty(1-\alpha_0)^{n-1}\sqrt{-G_0\rho}}$$

and

$$-2N = \frac{H_0''}{v_\infty(1-\alpha_0)^{n-1}},$$

where $H(\alpha) = -\alpha^2(1-\alpha)^2\rho g/B(\alpha)$ and prime denotes differentiation with respect to α.

We are interested in studying numerically the nonlinear stability of (2). First, in Section 2, we discuss the mathematical background of the problem. This includes the linear stability of (2) and a brief description of the nonlinear analysis given by Ganser and Drew [3, 4]. The understanding of the problem provided in Section 2

is central to the development of the numerical techniques required to solve (2) and to interpret the numerical results. It will be shown that, in some cases, periodic initial conditions with sufficiently long wavelengths, which are linearly unstable, are nonlinearly stable with respect to certain perturbations.

In Section 3, stable and accurate numerical methods are developed for the approximation of (2) together with periodic initial data. It is found that reductions in the time step may introduce instabilities unless the spatial grid size is sufficiently small. A similar phenomenon, also arising in a two-phase flow problem, is discussed in Lyczkowski, Gidaspow, Solbrig, and Hughes [8] and is attributed to the presence of complex characteristics, which is not the case here. Equation (2) thus provides a stringent test for a numerical algorithm; physical and numerical instabilities must be correctly distinguished. Finally, in Section 4, the results of our numerical experiments are given.

2. Mathematical Background

The standard method for studying the linear stability of (2), with $a=0$, is to look for solutions of the form

$$\alpha(x, t) \sim e^{i(kx-\mu t)}. \tag{4}$$

Substitution of this into (2), with $a=0$, leads to an equation for the wave frequency,

$$\mu = \frac{-R_2^{-1}k^3 + v^2 c_{0+} c_{0-}^2 k^3 + ivc_{0-}k^2(c_{0+} + R_2^{-1}k^2)}{1 + v^2 c_{0-}^2 k^2}. \tag{5}$$

A stable solution exists provided Im $\mu < 0$. Since $R_2^{-1} > 0$ and $c_{0-} < 0$, it is clear that all waves of the form given by (4) are stable (amplitudes decay to zero) if $c_{0+} > 0$. The sign of c_{0+} depends on α_0, the equilibrium value of the particle concentration. Examination of the definition for c_{0+} given in (3), yields the regions of stability shown in Fig. 1. All wavelengths decay to zero for $\alpha_0 > \alpha_0^u$ (stable states), only the larger wavelengths (small wave numbers) grow for unstable α_0 states. This is seen in Fig. 2 where Im μ is plotted as a function of wavelength. Note that, since we have scaled length with L, it is equivalent to set $k=1$ and let $1/L$ be the wave number. The neutrally stable wavelength is given by

$$R_{20}^{-1} = -c_{0+} \qquad \text{or} \qquad L_0 = L_1/\sqrt{-c_{0+}}, \tag{6}$$

where the subscript 0 denotes that L has been replaced by L_0 in the definition of R_2^{-1}. Since we want to include L_0 in the long wave approximations which gave rise to (2), it is necessary that $|c_{0+}| \ll 1$. This restricts our study of unstable α_0 states to those sufficiently close to α_0^u (see Fig. 1).

It is clear that, within linear theory, an initial condition of the form e^{ix} will grow

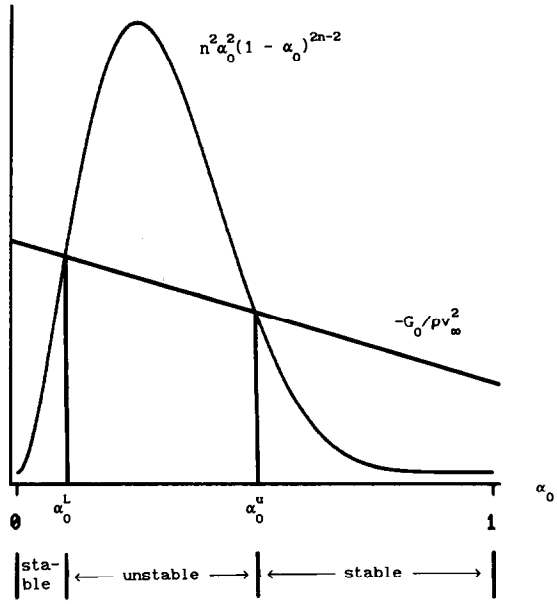

FIG. 1. Regions of stability and instability of α_0 states.

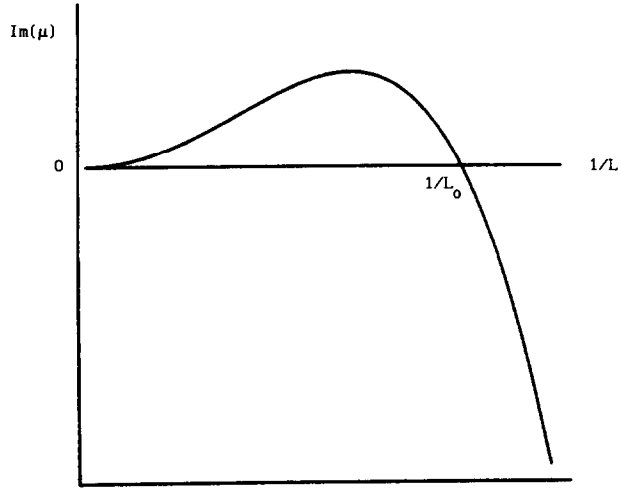

FIG. 2. Im μ plotted as a function of wave number $1/L$.

in amplitude indefinitely if $L > L_0$. If we are to continue to study the implications of the original mathematical model it is necessary to include nonlinear effects ($a \neq 0$).

For L close to L_0, and small amplitudes, the primary balance in (2) is

$$\alpha_t + R_2^{-1} \alpha_{xxx} \sim 0 \tag{7}$$

suggesting that time be rescaled by $\tilde{t} = R_2^{-1} t$. Equation (2) then becomes

$$\alpha_{\tilde{t}} + \beta(\alpha^2)_x + \alpha_{xxx} + \frac{\gamma}{2}(\alpha^2)_{xx} + \varepsilon\alpha_{xx} - \delta\alpha_{\tilde{t}x} = 0, \tag{8}$$

where

$$\begin{aligned} \beta &= -Na/R_2^{-1} \\ \varepsilon &= \frac{L_c c_{0+} c_{0-}}{L R_2^{-1}} \\ \gamma &= \frac{L_c a \tilde{c}_{0+} c_{0-}}{L R_2^{-1}} \\ \delta &= -L_c c_{0-}/L. \end{aligned} \tag{9}$$

Ganser and Drew [4] show that, for L close to L_0, an initial condition of the form $\alpha(x, 0) = \cos x$ evolves to

$$a\alpha = \frac{3mc_{0+}}{4N} \cos[x + \tilde{t}(1 + O(m^2)) - \theta_0] + o(m), \tag{10a}$$

where

$$r^2 = (L/L_0)^2 = 1 - \frac{9m^2}{64}\left(\frac{2}{3} + \frac{\tilde{c}_{0+}}{N}\right). \tag{10b}$$

From (10b) it is seen that the restriction L close to L_0 implies that m is small. Equations (10), therefore, imply that for a sufficiently small resulting m, an initial sinusoidal wave with wavelength $L > L_0$ (and thus linearly unstable) will evolve to a travelling wave with amplitude $3mc_{0+}/4N$ if $(-\tilde{c}_{0+}/N) > \frac{2}{3}$, where m is determined from (10b) for the given L. If $(-\tilde{c}_{0+}/N) < \frac{2}{3}$, the wave will continue to grow and, therefore, the α_0 state is nonlinearly unstable. On the other hand, if $(-\tilde{c}_{0+}/N) < \frac{2}{3}$, initial waves with $L < L_0$ will decay to zero if the initial amplitude is smaller than the critical amplitude given by (10b) and grow if it is larger. The solid curves in Fig. 3 show these different cases.

A way to extend this result for L not necessarily close to L_0 is to note that the

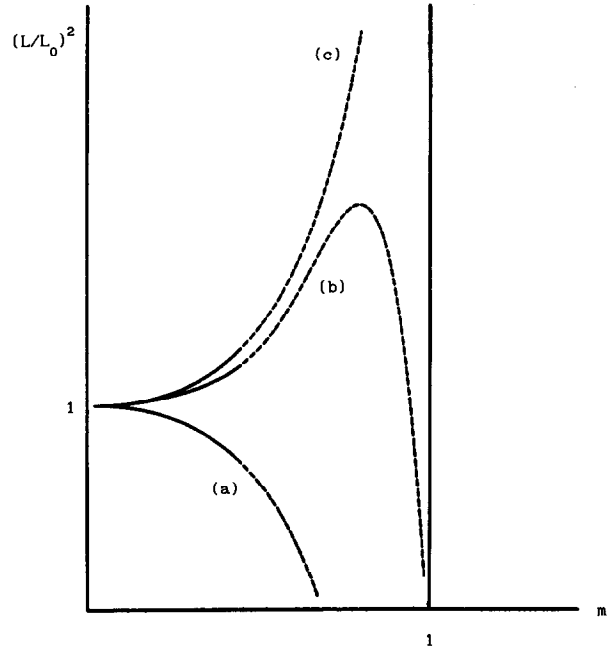

FIG. 3. Three representative cases for periodic solutions: (a) $(-\tilde{c}_{0+}/N) < \frac{2}{3}$; (b) $\frac{2}{3} < (-\tilde{c}_{0+}/N) < \frac{7}{6}$; (c) $(-\tilde{c}_{0+}/N) > \frac{7}{6}$.

equilibrated solution given in (10a) is a simple travelling wave. We, therefore, look for periodic solutions of (8) of the form $\alpha(\zeta) = \alpha(x - V\tilde{t})$. This gives

$$0 = -V\alpha_\zeta + \beta(\alpha^2)_\zeta + \alpha_{\zeta\zeta\zeta} + \frac{\gamma}{2}(\alpha^2)_{\zeta\zeta} + \varepsilon\alpha_{\zeta\zeta} + V\delta\alpha_{\zeta\zeta}. \tag{11}$$

Since the periodic initial conditions used to arrive at (10) also had an average value of zero over one period, we require further that solutions of (11) satisfy

$$\int_0^{2\pi} \alpha \, d\zeta = 0. \tag{12}$$

In Ganser and Drew [3], periodic solutions of (11) subject to (12) are found using perturbation techniques. These solutions are

$$a\alpha = \frac{-3mc_{0+}}{2Nf(m)}\left(\frac{(m-1)K + E}{mK} - cn^2\left(\frac{K}{\pi}(\zeta - \phi_0); m\right)\right) \tag{13a}$$

$$r^2 = (L/L_0)^2 = \frac{4K^2}{\pi^2} f(m), \tag{13b}$$

where $\zeta = x - (4K^2/\pi^2)\,(2 - m - 3E/K)\,\tilde{t}$. The terms $K(m)$ and $E(m)$ are the complete elliptic integrals of the first and second kind, respectively, and are functions

of the parameter m ($0 \leqslant m \leqslant 1$). The function $f(m)$ also involves elliptical functions, as well as parameters from the differential equation.

The important point is that for $m \to 0$, (13) reduces to (10) and, therefore, is an extension of the previous work. These additional results are shown in Fig. 3 as the dotted lines. Note that for case (c) ($-\tilde{c}_{0+}/N > \frac{7}{6}$) as $L \to \infty$, $m \to 1$ and the solution (13a) approaches a solitary wave.

This concludes the description of the mathematical results pertinent to the numerical work undertaken in the next two sections. For a complete discussion of the theory, see Ganser and Drew [3, 4].

3.1. *Discretization in Space and Time*

We wish to approximate solutions of (8) (tilde dropped for simplicity)

$$L(\alpha) = \alpha_t + \beta(\alpha^2)_x + \alpha_{xxx} + \frac{\gamma}{2}(\alpha^2)_{xx} + \varepsilon\alpha_{xx} - \delta\alpha_{tx} = 0, \tag{14a}$$

where $(x, t) \in [0, 2\pi] \times [0, \infty)$, constants β, γ, ε are defined by (9), subject to the initial data

$$\alpha(x, 0) = f(x) \qquad 0 \leqslant x \leqslant 2\pi \tag{14b}$$

and boundary conditions

$$\begin{aligned} &\alpha(0, t) = \alpha(2\pi, t), \qquad \alpha_x(0, t) = \alpha_x(2\pi, t), \\ &\alpha_{xx}(0, t) = \alpha_{xx}(2\pi, t), \qquad t > 0. \end{aligned} \tag{14c}$$

Since we restricted ourselves to periodic initial data in Section 2, it is sufficient to consider the initial/boundary value problem (14).

To discretize (14a) in space, a Petrov–Galerkin finite element method is used. Multiply through by $v(x)$, a twice differentiable function, and integrate by parts twice to obtain

$$\begin{aligned} &(\alpha_t, v) + \beta((\alpha^2)_x, v) + (\alpha_x, v_{xx}) - \frac{\gamma}{2}((\alpha^2)_x, v_x) - \varepsilon(\alpha_x, v_x) \\ &\quad - \delta(\alpha_{tx}, v) = 0, \end{aligned} \tag{15}$$

where $(\ ,\ )$ denotes the usual L_2 inner product

$$(f, g) = \int_0^{2\pi} f(x)\, g(x)\, dx.$$

Introduce a grid $0 = x_0 < x_1 < \cdots < x_p = 2\pi$ in space with uniform spacing $h = 2\pi/p$ and approximate the exact solution by

$$\alpha(x, t) \sim \sum_{i=0}^{p} A_i(t)\, \phi_i(x). \tag{16}$$

The presence of only first space derivatives in (15) means that the basis functions $\phi_i(x)$ can be chosen to be the usual C^0 linear hat functions having a support of $2h$.

The unknown functions $A_i(t)$ are obtained by solving the system of ordinary differential equations in t, given by

$$(A_t, \psi_j) + \beta((A^2)_x, \psi_j) + (A_x, (\psi_j)_{xx}) - \frac{\gamma}{2}((A^2)_x, (\psi_j)_x)$$
$$- \varepsilon(A_x, (\psi_j)_x) - \delta(A_{tx}, \psi_j) = 0, \tag{17}$$

$j = 0, 1, ..., p$ for suitable test functions $\psi_j(x)$ and initial data from (14b). The function $A_i(t) = A(x_i, t)$ approximates $\alpha(x_i, t)$. Rather than compute (17) in the standard fashion, we make use of the product approximation (Christie, Griffiths, Mitchell, and Sanz-Serna [1])

$$\alpha^2(x, t) \sim \sum_{i=0}^{p} A_i^2(t)\, \phi_i(x) \tag{18}$$

to handle the two nonlinear terms.

The test functions $\psi_j(x)$ are selected to be the C^2 Schoenberg cubic splines having a four element support and given by

$$\psi_j(x) = \frac{1}{6}\left[\left(\frac{x}{h} - j + 2\right)_+^3 - 4\left(\frac{x}{h} - j + 1\right)_+^3 + 6\left(\frac{x}{h} - j\right)_+^3 \right.$$
$$\left. - 4\left(\frac{x}{h} - j - 1\right)_+^3 + \left(\frac{x}{h} - j - 2\right)_+^3\right] \tag{19}$$

where $j - 2 \leqslant x/h \leqslant j + 2$ and

$$(x)_+ = \begin{cases} x & \text{if } x \geqslant 0 \\ 0 & \text{if } x \leqslant 0. \end{cases}$$

This procedure was used successfully by Sanz-Serna and Christie [11] to solve the KdV equation.

Substitution of (16), (18), and (19) into (17) yields the following autonomous system of ordinary differential equations ($\cdot \equiv d/dt$)

$$L_h(A) = \left(\frac{1}{120} + \frac{\delta}{24h}\right)\dot{A}_{j-2} + \left(\frac{13}{60} + \frac{5\delta}{12h}\right)\dot{A}_{j-1} + \frac{11}{20}\dot{A}_j + \left(\frac{13}{60} - \frac{5\delta}{12h}\right)\dot{A}_{j+1}$$
$$+ \left(\frac{1}{120} - \frac{\delta}{24h}\right)\dot{A}_{j+2} - \frac{\beta}{24h}(A_{j-2}^2 + 10A_{j-1}^2 - 10A_{j+1}^2 - A_{j+2}^2)$$
$$- \frac{1}{2h^3}(A_{j-2} - 2A_{j-1} + 2A_{j+1} - A_{j+2})$$
$$+ \frac{\gamma}{12h^2}(A_{j-2}^2 + 2A_{j-1}^2 - 6A_j^2 + 2A_{j+1}^2 + A_{j+2}^2)$$
$$+ \frac{\varepsilon}{6h^2}(A_{j-2} + 2A_{j-1} - 6A_j + 2A_{j+1} + A_{j+2}) = 0, \tag{20}$$

$j = 1, 2, ..., p$ with $A_j = A(x_j, t)$. The initial conditions are provided by (14b) and end values are found by imposing periodicity.

Taylor series expansions of (20) produce

$$L_h(\alpha) - L(\alpha) = \frac{h^2}{4} \frac{\partial^2}{\partial x^2} L(\alpha) + O(h^4)$$

which, upon using (14a), shows that (20) is fourth-order accurate in space when regarded as a finite difference scheme. The use of a piecewise linear interpolant to derive (20) clearly indicates that it is not fourth order over the entire spatial domain. However, this result is interesting since the usual Galerkin approach, without product approximation (18), leads only to second-order accuracy in space when it too is regarded as a finite difference scheme. The improvement in accuracy of product approximation over the standard Galerkin approach was noticed by Sanz-Serna and Christie [11] for the KdV equation. Equation (14a) reduces to the KdV equation when $\gamma = \varepsilon = \delta = 0$. Clearly, the replacement of the α^2 terms in (14a) by more general nonlinear functions will not reduce the fourth-order accuracy obtained by product approximation. An additional feature is that the system (20) is simpler than that produced by the standard Galerkin method and, therefore, it is less expensive computationally.

We write (20) in the form

$$M\dot{\mathbf{A}} = K\mathbf{A} + \mathbf{g}(\mathbf{A}) = \mathbf{F}(\mathbf{A}), \tag{21}$$

where $\mathbf{A}^{\mathrm{T}} = (A_1, A_2, ..., A_p)$, M and K are constant $p \times p$ matrices found in an obvious manner from (20) and $\mathbf{g}(\mathbf{A})$ contains the nonlinear terms in (20). The integration of (21) presented some difficulty. Our first attempt was to use the trapezoidal rule which gives second accuracy in time. However, instability was often present and we discarded the method. We turned next to the backwards Euler method which is only first-order accurate in time but is known to have better stability properties than the trapezoidal rule (see Lambert [6], for example). Although this led to an improvement, instability still remained for sufficiently small time steps. This unusual behaviour is discussed in Section 3.2. The low order of the backwards Euler proved to be inadequate so instead we implemented a second-order backwards differentiation formula (Lambert [6, p. 242]). This takes the form

$$M\left(\frac{3\mathbf{A}^{n+2} - 4\mathbf{A}^{n+1} + \mathbf{A}^n}{2\Delta t}\right) = \mathbf{F}(\mathbf{A}^{n+2}), \tag{22}$$

where $n = 0, 1, ...$ denotes the time level, Δt is the uniform time step and $A_j^n = A(x_j, n\Delta t)$. This 3-level scheme requires a second-order estimate for $\mathbf{A}_1$ and this was provided by the trapezoidal rule which did not exhibit instability until later time levels.

The system (22) is solved iteratively by Newton's method with the solution at the previous time level providing the starting estimate. Iteration continues until the

maximum norm of the difference between two successive iterates is less than a prescribed tolerance. The Jacobian is a 5-band matrix with three elements in the top right and bottom left corners coming from the periodicity conditions. Updating is required at each iteration and the linear system is solved by Gaussian elimination with the matrix being stored in nine vectors.

An alternative iteration of (22) was also considered where the linear and nonlinear terms of $\mathbf{F}(\mathbf{A})$, as shown in (21), are separated to give

$$\left(\frac{3}{2\Delta t}M - K\right)\mathbf{A}^{n+2} = M\left(\frac{1}{2\Delta t}(4\mathbf{A}^{n+1} - \mathbf{A}^{n})\right) + \mathbf{g}(\mathbf{A}^{n+2}). \tag{23}$$

The left-hand matrix is then constant, has the structure of the Jacobian described above, and can be factored once at the beginning, the pivots being stored for later use. The scheme (23) can be solved via a predictor-corrector approach. Unfortunately, this technique required a significantly larger number of iterations at each time step than Newton's method and it was decided, therefore, to use Newton's method throughout.

The time step Δt was held constant in each of our calculations. One reason for avoiding a variable time stepping procedure is that whenever Δt is reduced with h remaining fixed, instability often appears. This peculiar behaviour is now examined.

3.2. *Stability*

When solving systems of the type (21), it was found that satisfactory answers could be obtained for certain choices of Δt and h. On reducing Δt and keeping h fixed, however, instabilities appeared. This behaviour would usually be associated with an unstable numerical method. Numerical experiments demonstrated the phenomenon with several numerical schemes based on both Galerkin and finite difference approaches and a variety of time stepping techniques including backward differentiation formulas. We conjectured that a positive lower bound stability restriction on $\Delta t/h^2$ must be present.

As an illustration of the stability properties we consider the linear equation

$$\alpha_t + \alpha_{xxx} + \varepsilon\alpha_{xx} - \delta\alpha_{txx} = 0, \tag{24}$$

where ε and δ are positive constants. Discretize in space by Galerkin's method with piecewise linear trial and test functions except for α_{xxx} which is given its usual 5-point replacement. Discretize in time by the backwards Euler method to give

$$\begin{aligned}&\frac{1}{6h\Delta t}(h+3\delta)(A_{m-1}^{n+1} - A_{m-1}^{n}) + \frac{2}{3\Delta t}(A_m^{n+1} - A_m^{n})\\ &\quad + \frac{1}{6h\Delta t}(h-3\delta)(A_{m+1}^{n+1} - A_{m+1}^{n}) - \frac{1}{2h^3}(A_{m-2}^{n+1} - 2A_{m-1}^{n+1} + 2A_{m+1}^{n+1} - A_{m+2}^{n+1})\\ &\quad + \frac{\varepsilon}{h^2}(A_{m-1}^{n+1} - 2A_m^{n+1} + A_{m+1}^{n+1}) = 0,\end{aligned} \tag{25}$$

where $m = 1, 2, ..., p$ and $n = 0, 1, ...$ This discretization is different from that described earlier and used to produce the numerical results which appear later. However, its stability analysis is simpler and it serves as a useful illustration of an instability phenomenon which was observed in a large number of numerical methods.

We apply the von Neumann stability test (see Mitchell and Griffiths [9]) to (25) by substituting the general Fourier component

$$A_m^n \sim \xi^n e^{ikmh},$$

where k is the wave number and $i = \sqrt{-1}$. For stability, we require that either $(|\xi|^2 - 1)/\Delta t$ is negative or, if positive, that it be bounded by a constant M, independent of Δt and h. Now

$$\frac{|\xi|^2 - 1}{\Delta t} = \frac{\begin{bmatrix} 12(1-\cos Q)[\varepsilon h^2(2+\cos Q) - 3\delta \sin^2 Q \\ \quad - 3\varepsilon^2 r h^2(1-\cos Q) - 3r \sin^2 Q(1-\cos Q)] \end{bmatrix}}{h^4[2+\cos Q + 6\varepsilon r(\cos Q - 1)]^2 + 9h^2 \sin^2 Q[2r(\cos Q - 1) - \delta]^2}, \tag{26}$$

where $r = \Delta t/h^2$ and $Q = kh$. First we consider $Q = \pi$:

$$\frac{|\xi|^2 - 1}{\Delta t} = \frac{24\varepsilon[1 - 6\varepsilon r]}{h^2[1 - 12\varepsilon r]^2}.$$

It follows that, unless $r \geqslant 1/(6\varepsilon)$, $(|\xi|^2 - 1)/\Delta t$ is unbounded as $h \to 0$. Hence, it is necessary that

$$r \geqslant 1/6\varepsilon \tag{27}$$

for stability.

We can show that (27) is also sufficient for stability. Denote the numerator of (26) by $12(v - w)$, where

$$\begin{aligned} v(Q) &= (1 - \cos Q)[\varepsilon h^2(2 + \cos Q) - 3\delta \sin^2 Q] \\ w(Q) &= 3r(1 - \cos Q)^2[\varepsilon^2 h^2 + \sin^2 Q]. \end{aligned} \tag{28}$$

Analysis of $v(Q)$ for $h \ll 1$ reveals two regions in $[0, 2\pi]$, where v is non-negative; $[0, h\sqrt{\varepsilon/\delta}]$ and $[\pi - \alpha, \pi + \alpha]$, where $0 < \alpha < \pi/2$. On the other hand, $-w(Q)$ is negative on $(0, 2\pi)$ and zero at $Q = 0, 2\pi$. Between $\pi/2$ and $3\pi/2$ the largest value of $-w$ is $-12r\varepsilon^2$ taken only at $Q = \pi$. Hence, by examining $v(\pi) - w(\pi)$ we see that, if (27) is satisfied, $v - w$ is negative except possibly on $[0, h\sqrt{\varepsilon/\delta}]$. Expansion of $v(Q) - w(Q)$ for $Q \ll 1$ yields

$$v(Q) - w(Q) = \frac{Q^2 h^2}{2}[3\varepsilon - 3\delta Q^2/h^2 + O(Q^2, Q^4/h^2, rQ^2, rQ^4/h^2)]. \tag{29}$$

This will remain positive for Δt and h sufficiently small. This must be the case for a consistent numerical algorithm since the above expression with $Q \ll 1$ (or $h \ll 1$, k fixed) corresponds to the continuous problem where small wave numbers are unstable (see Eq. (5)). Expanding the denominator of (26) for Q small shows that $|\xi|^2 \leqslant 1 + M\,\Delta t$, where M is a constant independent of Δt and h. The stability requirement is now satisfied for all Q when Δt and h are sufficiently small and satisfy (27).

4. Numerical Results

The results presented here are based on the parameter values $N = 0.05$, $L_1 = 10^{-5/2}$, $L_c = 0.001$, $c_{0+} = -0.0025$, $c_{0-} = -4$, $\tilde{c}_{0+} = -1$ and, in light of (13a), we normalize the size of the perturbation by choosing $a = c_{0+}\, c_{0-}$. This choice ensures that we are considering the case (c) shown in Fig. 3. We are particularly interested in whether given initial data (14b) for Eq. (14a) will, for a given r (defined by (10b)) evolve into travelling wave solutions corresponding to solutions of the ordinary differential equation (11). The problem (11), (12), and periodic boundary data was solved numerically by a second-order finite difference method on a uniform mesh of width $h = 2\pi/100$. The integral term (12) was approximated by the trapezoidal rule and the resulting system of algebraic equations was solved by Newton's method. Continuation was used to advance the solution from $r = 1.01$ to $r = 20$. In Fig. 4, graphs of $r = 1.01$, 1.5, 5, and 20 demonstrate that, as r increases, the solution changes from a basic sine wave into a solitary wave. Note

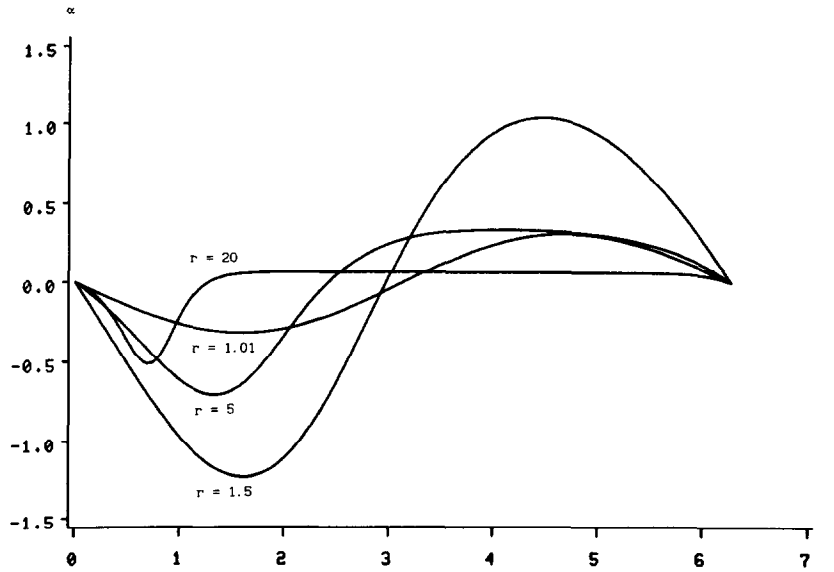

FIG. 4. Solutions of (11) with various r showing the development of a solitary wave.

TABLE I

r	Maximum	Minimum
1.01	0.311	−0.318
1.5	1.041	−1.233
2	0.876	−1.139
5	0.338	−0.706
10	0.147	−0.565
15	0.091	−0.527
20	0.066	−0.511

that the solutions in Fig. 4 agree with the theoretical results (10) and (13). For example, at $r = 1.01$ the predicted amplitude from (10) is 0.322, whereas the numerical solution gives $-0.318 \leqslant \alpha \leqslant 0.311$. The minimum value of the solution occurs close to $r = 1.5$. Some of the maximum and minimum values of the solution at different r values are given in Table I. A graph of the minimum values against r is shown in Fig. 5.

Turning now to the partial differential equation, problem (14), we choose $f(x) = 0.1 \sin x$ to represent a small initial disturbance. The method of solution is (22) which is second order in time and fourth order in space. This scheme is iterated by Newton's method and, typically, between two and four iterations are required for 10-decimal place accuracy. The Newton iteration is started by taking the initial estimate to be the solution computed at the previous time level.

First we run the case $r = 1.5$ for which the coefficients in (14a) given by (9) are approximately $\beta = -0.45$, $\gamma = 0.37947$, $\delta = 0.04216$, and $\varepsilon = 0.09487$. With the number of elements $p = 200$ and the time step $\Delta t = 0.01$ a minimum of -1.230 is obtained at $t = 100$. In Fig. 6 the evolution of the solution is shown for $t = 20$, 40,

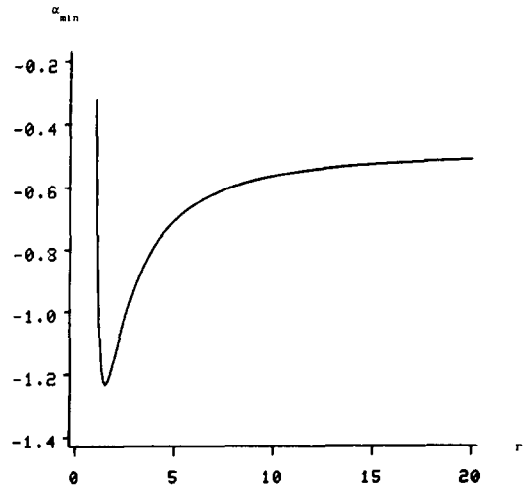

FIG. 5. Plot of minimum values of α ($\alpha_{\min}$), computed from (11), for $1.01 \leqslant r \leqslant 20$.

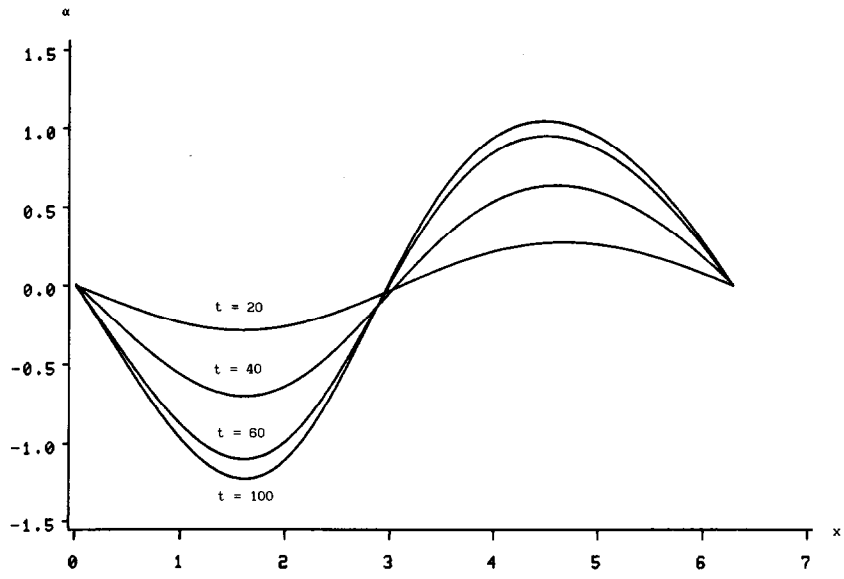

FIG. 6. Solution of (14) with $r = 1.5$ at various time levels, shifted to show zero end values.

60, and 100. By $t = 100$ the fully developed travelling wave solution has been obtained. In order to compare amplitudes at different time levels, since the wave is moving, we have shifted each solution so that $\alpha(0) = \alpha(2\pi) = 0$. If we now set $\Delta t = 0.001$ then instability occurs which can be overcome by an appropriate increase in p, as is discussed in Section 3.2.

Several other cases with different values of r also are computed. For r close to one, the growth rate of the solution into a travelling wave is slow and hundreds of thousands of time steps are required. We performed experiments with r as small as 1.01 and again found agreement with the solution of (11). For $r < 1$ the solution was found to decay to zero, as predicted by the theory in Section 2. For $1.0 \leqslant r \leqslant 2.4$ the behaviour of the solution is much the same as the $r = 1.5$ case. At $r = 2.5$, however, an interesting phenomenon occurs. Rather than evolving to the travelling wave solution with period 2π, the solution evolves to a travelling wave with period π and is shown in Fig. 7. This solution with $p = 200$ and $\Delta t = 0.01$ is fully developed by $t = 120$ and was verified numerically to be a solution of (11). A simple change of variable shows that this solution with period π for $r = 2.5$ is identical to the solution of (11) with period 2π for $r = 1.25$. Near linear theory (see Ganser and Drew [4]) suggests that the first harmonic which is generated by the nonlinearities and is dispersing at a different speed than the fundamental period, begins to dominate at $r = 2.5$. We note that for $r < 2$ the first harmonic decays to zero for sufficiently small amplitudes (as is the case here) and only begins to grow for $r > 2$. Evidently the first harmonic only begins to dominate at $r = 2.5$.

Continuing to increase, r shows that the first harmonic dominates and the initial

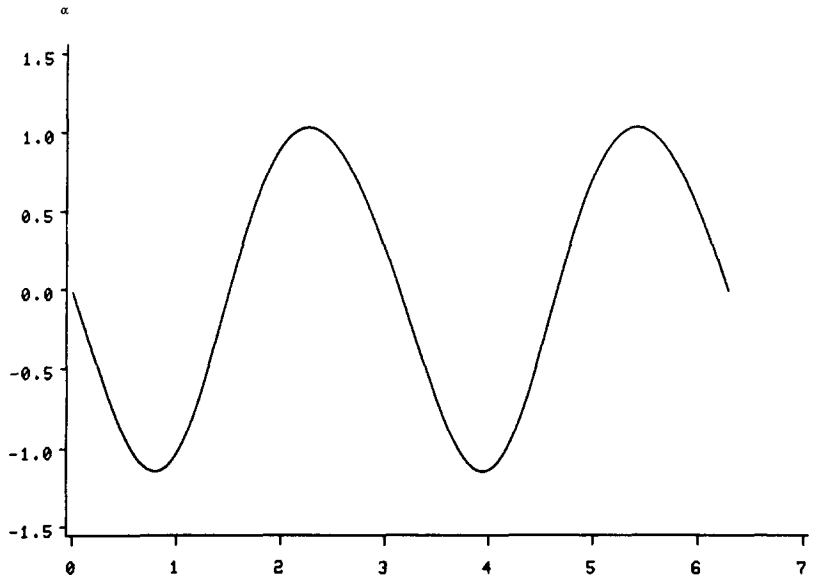

FIG. 7. Solution of (14) with $r = 2.5$ at $t = 120$, showing the presence of a second hump.

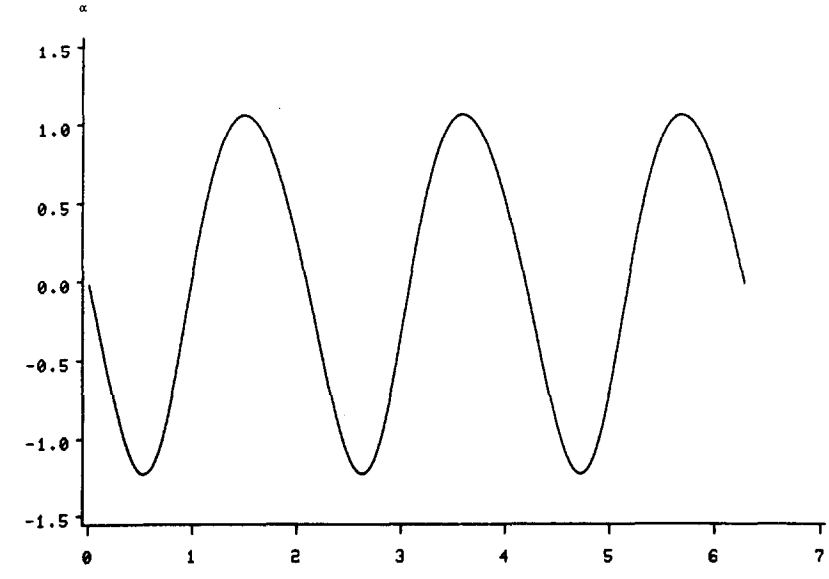

FIG. 8. Solution of (14) with $r = 4.3$ at $t = 40$, showing the presence of a third hump.

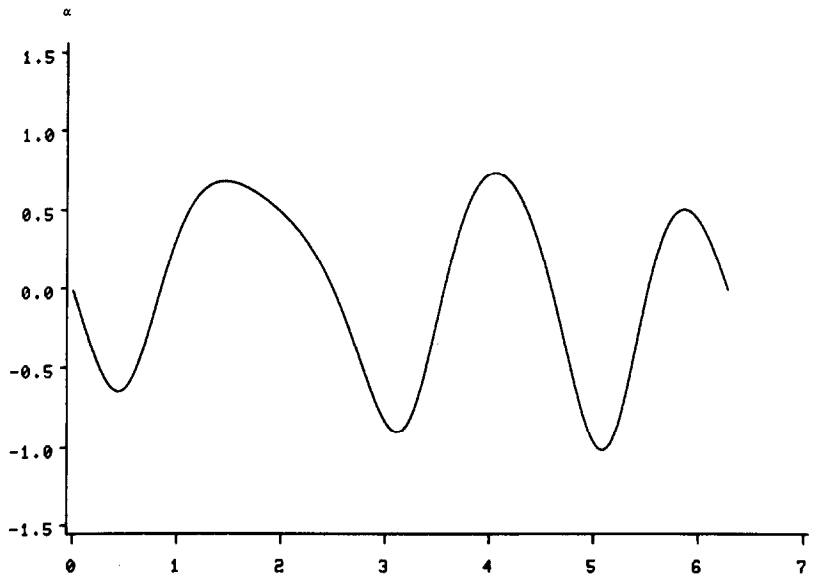

FIG. 9. Solution of (14) with $r = 6.4$ at $t = 3$, showing the evolution of the fourth hump.

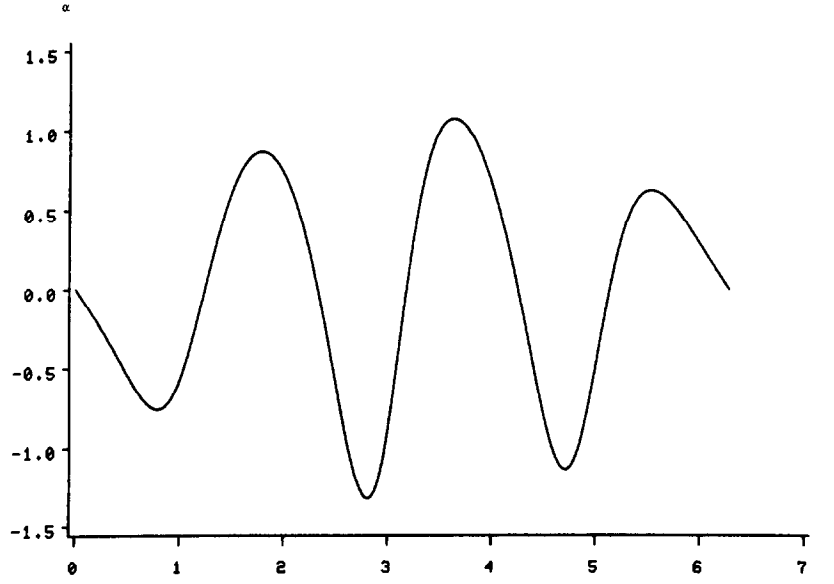

FIG. 10. Solution of (14) with $r = 6.4$ at $t = 6$, showing the evolution of the fourth hump.

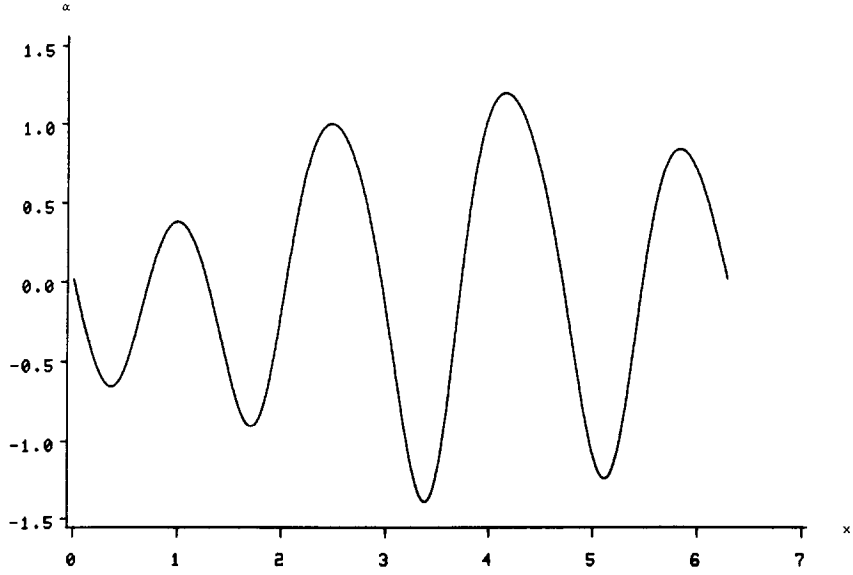

FIG. 11. Solution of (14) with $r = 6.4$ at $t = 9$, showing the evolution of the fourth hump.

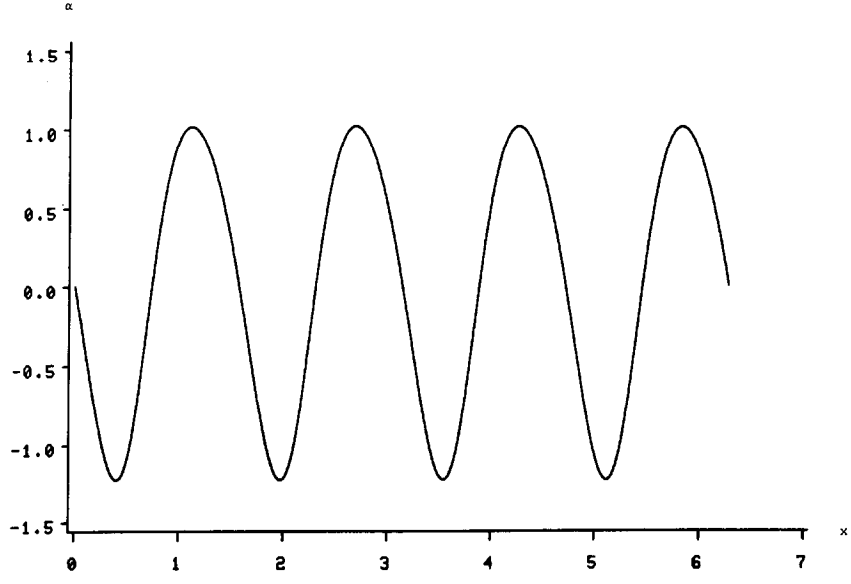

FIG. 12. Solution of (14) with $r = 6.4$ at $t = 12$, showing the evolution of the fourth hump.

condition evolves to a solution of (11) corresponding to $r/2$ until about $r = 4.2$. At $r = 4.3$ the fully developed travelling wave now has period $2\pi/3$ and corresponds to a solution of (11) with $r/3$. This solution is shown in Fig. 8 and is obtained with $p = 400$, $\Delta t = 0.001$ at $t = 40$. A finer mesh is required in this case and at higher transition regions: Too coarse a mesh may affect which is the controlling harmonic.

Notice that, as r increases, the growth rate increases and the travelling wave is reached sooner. The third harmonic begins to dominate at $r = 6.4$ with $p = 400$, $\Delta t = 0.001$, $t = 15$ and the fourth hump appears for a value of r between 8.7 and 8.8 depending on the mesh. This behaviour apparently continues as r is increased.

As a final case we present results in Figs. 9 through 12 showing the evolution of the "fourth hump" at $r = 6.4$. These solutions with $p = 400$, $\Delta t = 0.001$ are at time levels $t = 3$, 6, 9, and 12, and the minimum at $t = 12$ is -1.224. The fourth hump appears between $t = 3$ and $t = 6$. Prior to "settling down" at $t = 12$, the solutions at $t = 3$ and 6 show a beat-like appearance caused by the competing mode interactions.

5. Concluding Remarks

The numerical calculations have given a verification of the formal perturbation analysis done by Ganser and Drew and an increased confidence in both approximation procedures. With this confirmation in mind, it is possible to make progress numerically in the understanding of the mathematical model when the analytic techniques become difficult. The numerical discovery of the dominance of the higher harmonics for initial conditions with sufficiently long wavelengths ($r \geqslant 2.5$) is an example of this.

The numerical instability introduced by a reduction of the time step posed a problem. All of the schemes which we used to solve the equation exhibited this behaviour, some more severely than others. A stability analysis of a simplified case, together with an understanding of the mathematical model led us to conclude that this instability at smaller time steps is acceptable. However, it seems that this feature would provide a considerable difficulty for an ODE package which, when estimating a large error, would attempt to decrease the time step rather than increase it, as might be required to satisfy a stability restriction.

The finite element method selected for the discretization in space gave fourth-order accuracy when product approximation was applied to the nonlinear terms. The resulting equations are simpler computationally than those obtained by the standard Galerkin scheme. This is an extension of the scheme devised by Sanz-Serna and Christie for the KdV equation.

The experience we have gained here will be directed now towards a greater understanding of the original system of equations by means of mathematical and numerical techniques.

ACKNOWLEDGMENTS

This research was supported in part by an appointment to the U.S. Department of Energy Faculty Research Participation Program administered by Oak Ridge Associated Universities.

REFERENCES

1. I. CHRISTIE, D. F. GRIFFITHS, A. R. MITCHELL, AND J. M. SANZ-SERNA, *IMA J. Num. Anal.* **1**, 253 (1981).
2. D. A. DREW, *Annu. Rev. Fluid Mech.* **15**, 261 (1983).
3. G. H. GANSER AND D. A. DREW, *SIAM J. Appl. Math.* **47**, 726 (1987).
4. G. H. GANSER AND D. A. DREW, submitted for publication.
5. G. M. HOMSY, M. M. EL-KAISSY, AND A. DIDWANIA, *Int. J. Multiphase Flow* **6**, 305 (1980).
6. J. D. LAMBERT, *Computational Methods in Ordinary Differential Equations* (Wiley, New York, 1973).
7. J. T. C. LIU, *Proc. Roy. Soc. London A* **389**, 331 (1983).
8. R. W. LYCZKOWSKI, D. GIDASPOW, C. W. SOLBRIG, AND E. D. HUGHES, *Nucl. Sci. Eng.* **66**, 378 (1978).
9. A. R. MITCHELL AND D. F. GRIFFITHS, *The Finite Difference Method in Partial Differential Equations* (Wiley, New York, 1980).
10. D. J. NEEDHAM AND J. H. MERKIN, *J. Fluid Mech.* **131**, 427 (1983).
11. J. M. SANZ-SERNA AND I. CHRISTIE, *J. Comput. Phys.* **39**, 94 (1981).